14th International Symposium on Turbulence and Shear Flow Phenomena (TSFP14)
Heidelberg, Germany, July 28–31, 2026

RELAMINARIZATION OF A TURBULENT FLOW ENTERING A ROTATING ANNULAR DUCT

Thomas Hultsch
Institute of Fluid Mechanics
Technische Universität Dresden
01062 Dresden
thomas.hultsch@tu-dresden.de

Jörg Stiller
Institute of Fluid Mechanics
Technische Universität Dresden
01062 Dresden
joerg.stiller@tu-dresden.de

Jochen Fröhlich
Institute of Fluid Mechanics
Technische Universität Dresden
01062 Dresden
jochen.froehlich@tu-dresden.de

ABSTRACT

The development of turbulent flow inside a rotating cavity is relevant for rotor internal cooling concepts in electric-vehicle drives, where rotation can simultaneously enhance and suppress turbulence. In this study, high-resolution large-eddy simulations are performed to investigate the relaminarization of a turbulent flow as it enters a rotating annular duct. The configuration consists of a turbulent pipe flow forming a jet in a cylindrical cavity before being redirected into an annular duct bounded by a rotating outer wall. Two cases are analyzed: a rotating configuration and a non-rotating reference case.

The simulations reveal that rotation significantly modifies the flow structure and turbulence characteristics. While turbulence is initially enhanced in the jet region due to strong shear near the rotating wall, it rapidly decays downstream as the flow enters the annular duct. Analysis of turbulent kinetic energy profiles shows a pronounced reduction of turbulence near the rotating wall, leading to complete relaminarization in the annular duct. Examination of turbulence production terms demonstrates that this behavior results from the disappearance of turbulence production mechanisms and the damping of radial velocity fluctuations by centrifugal forces. Visualization of vortex structures further confirms the rapid disappearance of near-wall turbulence in the rotating case.

These findings provide insight into the mechanisms governing relaminarization in rotating flows and contribute to the optimization of rotor internal cooling configurations.

INTRODUCTION

A promising approach for preventing high–power electric-vehicle drives from over-heating is rotor internal cooling. The present contribution considers a model configuration featuring the essential elements of such a device (Weber & Doerr, 2017). Turbulent pipe flow enters a larger cylindrical cavity inside the rotor, where it forms a jet. The flow is then redirected within the cavity and exits through an annular duct bounded by the stationary pipe wall on the inside and the rotating rotor wall on the outside. This creates a complex transitional flow in which opposing effects of the rotation lead to increased turbulence production and strong turbulence damping simultaneously. The basic effects of turbulence intensification and damping by flow rotation are known from simple configurations, such as a rotating pipe (Imao *et al.*, 1996; Nishibori *et al.*, 1987; Orlandi & Fatica, 1997). The present configuration is much more complex as it contains non-rotating and rotating parts and massive changes in cross-section.

A preliminary study of this flow was conducted by Hultsch *et al.* (2023), reporting a single case with rotation of the outer wall. Radial profiles of different components of the Reynolds stress tensor were analyzed in the jet region and the annular duct. It was found that the turbulence is characterized locally by strong anisotropy, with variation of the dominant component. Relaminarization occurs at the transition between the jet region and the annular duct, resulting in complete attenuation of the turbulent fluctuations near the rotating wall.

In the present contribution, the general structure of the flow and the turbulence properties are investigated for two cases: one with and one without rotation. New data from an improved simulation setup is analyzed, including an extended calculation of turbulence statistics. The development of turbulence along radial and axial profiles will be compared, with a focus on relaminarization in the transition area to the annular duct. Detailed knowledge of the dependence of local turbulence characteristics on rotation, provided by this study, is crucial for cooling applications, since the efficiency of cooling strongly depends on the turbulent heat transfer.

SETUP

Figure 1 shows the considered configuration, as described in Hultsch *et al.* (2023). The flow enters the domain through a stationary pipe with diameter d and a length of $L_\mathrm{p} = 15d$. Turbulence is initiated by a tripping force near the inlet (Schlatter & Örlü, 2012) and develops rapidly, so that fully developed turbulent pipe flow is obtained upstream of the pipe exit. The Reynolds number in the pipe is $Re_\mathrm{p} = dU_\mathrm{p}/\nu = 17640$. The cylindrical cavity has a length of $L_\mathrm{c} = 5d$ and a diameter of $D = 2R = (7/3)d$. The annular duct leading to the outlet of the domain has a width of $s = (7/12)d$ and a length of $L_\mathrm{a} = 12s$.

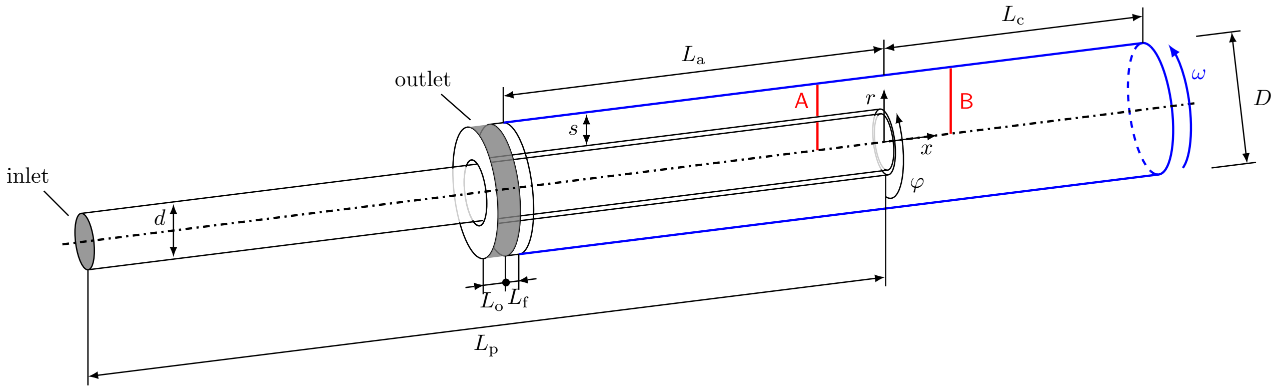

Figure 1: Simulation domain. Blue walls indicate rotation around the x-axis. The vertical red lines A and B mark the position of the first and last profile in Fig. 3.

The outlet of the domain is located in the outer wall at the end of the annular duct. Blue coloring indicates walls rotating around the x-axis. The ratio of the circumferential velocity of the wall to the bulk velocity in the pipe is $Ro = \omega R/U_\mathrm{p} = 2$ in the rotating case.

After reaching a statistically stationary flow, time averaging was started. The rotating flow was averaged over 51 revolutions of the rotor wall, corresponding to 11300 viscous time units of the pipe flow. The non-rotating flow was averaged in a comparable manner for 11800 viscous time units of the pipe flow.

NUMERICAL METHOD AND DISCRETIZATION

The simulations were performed with the spectral element-Fourier solver Semtex (Blackburn *et al.*, 2019), which integrates the incompressible Navier–Stokes equations in a cylindrical coordinate system (x, r, φ) within an axisymmetric domain. The meridional plane was discretized using 5253 elements with a polynomial degree of 10, ensuring full resolution of the wall boundary layers for the present physical parameters. In the circumferential direction, a Fourier expansion with 360 modes was applied. A third-order semi-implicit scheme was used for time integration.

To stabilize the solver and account for the smallest turbulent eddies, a spectral vanishing viscosity (SVV) approach was employed. In the circumferential direction, a novel locally adaptive SVV kernel was applied (Hultsch *et al.*, in prep.), based on the kernel modifications of Koal *et al.* (2012). In the meridional plane, the exponential kernel of Tadmor (1989), later adapted for the spectral element method by Maday *et al.* (1993), was used. For the flows simulated here, the SVV contribution was about 10.4 % of the total volume-averaged dissipation, while in some regions locally remaining of similar magnitude as the resolved dissipation. The maximum ratio of approximately 20 % occurs in the thin shear layer near the rotating wall in the jet region.

RESULTS

Flow structure

The mean velocity magnitude of the flow in the x-r-plane is shown in Fig. 2a and c for the non-rotating and the rotating case, respectively. The solution was averaged in time and in the circumferential direction for both cases. Two snapshots of the respective instantaneous flow are presented in Fig. 2b and 2d.

The basic flow structure is similar in both cases. When the turbulent flow leaves the inlet pipe, it forms a highly turbulent jet. The presence of the back end of the cavity slows down the jet. Furthermore, the fairly narrow outer wall of the cavity poses backflow, so that a strongly turbulent shear layer between the jet and the outer back flow is created, with considerable radial momentum exchange. As a result, only a small portion of the fluid reaches the back wall of the cavity, where it is deflected radially outward. A major portion of the fluid is already deflected between $x/L_\mathrm{c} = 0.25$ and 0.75 by the increasing pressure. After flow reversal in the cylindrical cavity, the fluid enters the annular duct towards the outlet. For geometrical reasons, the bulk velocity in the annular duct is $U_s = (12/49)U_\mathrm{p}$. The bulk Reynolds number in this part is $Re_s = sU_s/\nu = 2520$.

The rotation of the cavity wall introduces several important features. When the jet impinges on the back wall of the cavity, the fluid begins to rotate with the wall. Centrifugal forces drive the flow radially outward, enhancing the flow towards the back wall. An additional rotating boundary layer emerges near the rotating wall. In the jet region ($x \geq 0.25\,L_\mathrm{c}$), the rotating boundary layer remains very thin, as the incoming non-rotating fluid restricts its thickness. The turbulent shear layer of the jet induces strong momentum exchange of the rotating fluid with the non-rotating flow, producing a steep velocity gradient and enhanced turbulence generation near the rotating wall (Fig. 3).

Close to the pipe outlet (and annulus inlet), the influence of the jet diminishes, and the rotating boundary layer expands rapidly ($x \approx 0.2\,L_\mathrm{c}$). As a result, the centrifugal force of the rotating fluid increases the pressure at the outer wall. The axial flow directed toward the annular duct is then deflected radially inward by this high-pressure region, as illustrated by the streamlines in Fig. 2c. In the annular duct, the flow characteristics change fundamentally. The fluid in the entire cross-section rotates, while the axial bulk velocity reduces similarly to the non-rotating case. This results in a drastic decrease in turbulence, which is detailed in the following section.

Development of turbulence

Figure 3 shows radial profiles of turbulent kinetic energy (TKE) at characteristic locations in the transition region between $x/L_\mathrm{c} = -0.25$ and 0.25 for both the rotating ($Ro = 2$) and non-rotating ($Ro = 0$) cases. The first two profiles are in the annular duct and in the inlet pipe. The third is directly

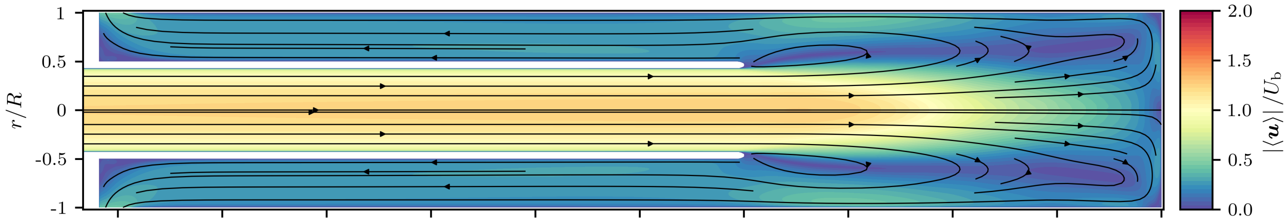

(a) $Ro = 0$: mean flow with streamlines

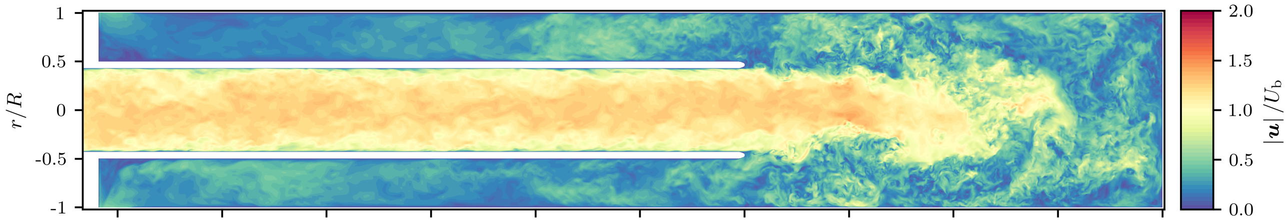

(b) $Ro = 0$: instantaneous flow

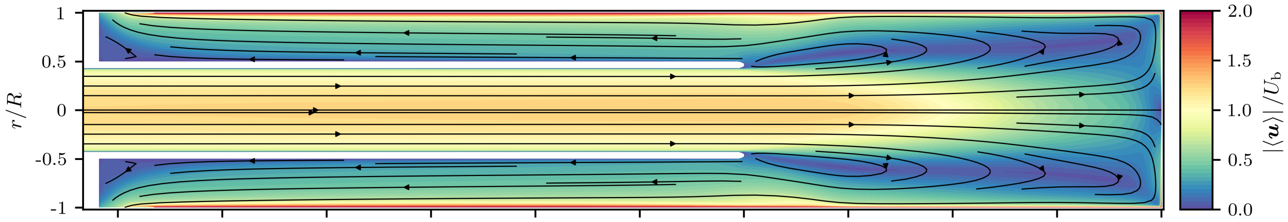

(c) $Ro = 2$: mean flow with streamlines

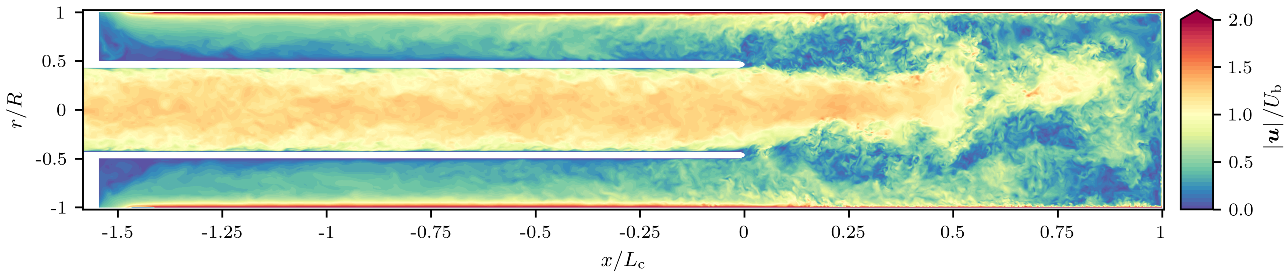

(d) $Ro = 2$: instantaneous flow

Figure 2: Flow in a meridional plane section of the domain. a) Streamlines and absolute value of mean velocity in non-rotating cavity, b) absolute value of instantaneous velocity in non-rotating cavity, c) same as a) for rotating cavity, d) same as b) for rotating cavity. Inflow pipe not shown.

adjacent to the end of the inlet pipe, and the last two profiles are in the jet region. Axial profiles in the outer part of the domain ($r/R > 0.41$) are shown in Fig. 4. The bottom profile ($r = 0.41$) starts within the inlet pipe; the other profiles are distributed across the annular duct and the outer part of the jet region.

The lower section of the two radial profiles at $x/L_c = -0.25$ and -0.125 displays the TKE of the entering pipe flow, with its maximum in the wall boundary layer at $r/R = 0.41$. Since rotation of the cavity wall does not affect the flow here, turbulence is essentially identical in both cases. The axial development of TKE at $r/R = 0.41$ is shown in the bottom profile of Fig. 4. Inside the pipe ($x < 0$), the turbulence level is constant because the flow is fully developed. In the jet shear layer, however, TKE increases by almost one order of magnitude and reaches its maximum at $x/L_c \approx 0.5$, with rotation causing a slight reduction. As the flow slows in the stagnation zone at the back wall, turbulence decreases along with the influence of rotation. Right at the back wall, $x/L_c = 1$, the velocity fluctuations vanish, but a thin shear layer is visible at this wall.

The TKE in the jet region is also illustrated by the radial profiles at $x/L_c = 0.125$ and 0.25 (Fig. 3). The maximum lies in the jet shear layer at $r/R \approx 0.45$. The damping effect of the rotation is limited to the outer part ($r/R > 0.4$) at $x/L_c = 0.125$, but eventually continues to the center of the domain at $x/L_c = 0.25$. Close to the rotating wall at $x/L_c = 0.25$, a second local maximum of TKE appears at $r/R \approx 0.98$. The steep gradient of the circumferential velocity inside this thin boundary layer drives intense turbulence production, outweighing the damping effect of rotation. As the rotating boundary layer grows, this local maximum moves radially inwards (see $x/L_c = 0.125$).

The axial development of TKE in the outer region of the domain leading to the annular duct is shown in the upper profiles of Fig. 4. At $r/R = 0.75$, which is the radial center of the annular duct, the TKE in the jet shear layer ($x > 0$) is reduced by the rotation, similar to $r/R = 0.41$. Inside the annular duct ($x < 0$), the TKE decreases gradually, with a generally lower level in the rotating case, due to the damping effect of the outer rotating wall.

The radial position of the topmost profile in Fig. 4 ($r/R = 0.98$) corresponds to the position of the local maximum of TKE near the rotating wall in the radial profile at $x/L_c = 0.25$.

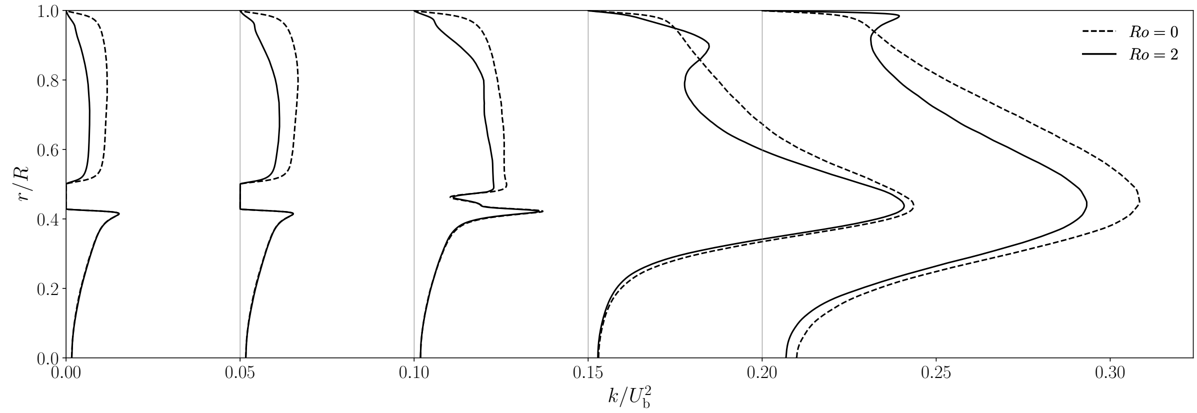

Figure 3: Radial profiles of TKE at different axial positions between line A and B in Fig. 1). From left to right: $x/L_c = \{-0.25, -0.125, 0.01, 0.125, 0.25\}$. Plotted profiles are shifted along the horizontal axis.

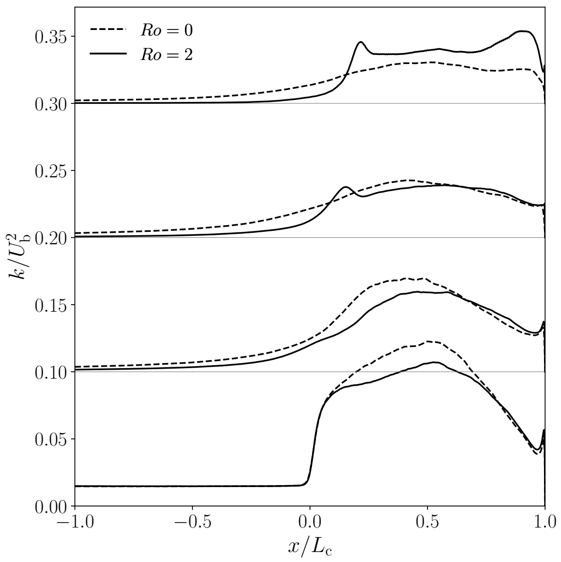

Figure 4: Axial profiles of TKE at different radial positions. From bottom to top: $r/R = \{0.41, 0.75, 0.9, 0.98\}$. Plotted profiles are shifted along the vertical axis.

This profile has three local maxima in the rotating case and only two in the non-rotating case. The local maximum at $x/L_c \approx 0.9$ results from radial flow along the back wall coming from the center of the domain and impinging on the outer wall. It is more pronounced in the rotating case because the radial flow is stronger due to the additional centrifugal force. The high TKE region around $x/L_c \approx 0.5$ reflects the jet shear layer. In the non-rotating case, the TKE gradually decreases as the flow enters the annular duct. A small amount of turbulence remains within the annular duct due to the wall boundary layer of the axial velocity. In the rotating case, turbulence decays much faster: between $x/L_c = 0.2$ and 0.1, the TKE drops by about one order of magnitude. The axial flow separates from the rotating wall as the rotating boundary layer expands, reducing turbulence production, while stronger rotation further damps radial fluctuations through centrifugal forces. Downstream in the annular duct, the TKE vanishes completely, and the flow relaminarizes.

This behavior is confirmed in the top section of the left two profiles in Fig. 3, showing the TKE in the annular duct. In the non-rotating case, turbulence increases slightly with radius. Under rotation, however, turbulence decreases considerably for $r/R > 0.8$ as the circumferential velocity rises towards the outer wall, where the flow eventually relaminarizes. In the inner half of the duct ($r/R \leq 0.75$), where rotational effects are weaker, turbulence is still significantly reduced compared to the non-rotating case.

Turbulence production near the outer wall

The sudden reduction of TKE near the rotating outer wall can be explained by the development of the production term P_k of the transport equation of TKE, which is given in cylindrical coordinates by

$$\begin{aligned} P_k = &-\langle u'u'\rangle \langle u\rangle_{,x} - \langle u'v'\rangle \langle u\rangle_{,r} - \langle u'w'\rangle \frac{\langle u\rangle_{,\varphi}}{r} \\ &-\langle u'v'\rangle \langle v\rangle_{,x} - \langle v'v'\rangle \langle v\rangle_{,r} - \langle v'w'\rangle \frac{\langle v\rangle_{,\varphi} - \langle w\rangle}{r} \\ &-\langle u'w'\rangle \langle w\rangle_{,x} - \langle v'w'\rangle \langle w\rangle_{,r} - \langle w'w'\rangle \frac{\langle w\rangle_{,\varphi} + \langle v\rangle}{r} \end{aligned} \quad (1)$$

Here, u, v and w are the velocity components in axial, radial and tangential direction, respectively. Averaging is denoted by $\langle \ldots \rangle$, and u', v', w' are the velocity fluctuations. Indices starting with a comma indicate derivatives in the respective direction.

Figure 5 presents axial profiles of the complete production term P_k together with four selected subterms at $r/R = 0.98$ in the transition region between $x/L_c = -0.35$ and 0.35. The production in the non-rotating case is much smaller than in the rotating case. In the jet region, it is even slightly negative, since turbulence is transported to the wall from the jet shear layer. The small amount of turbulence production in the annular region is caused by the second term of Eq. (1), which is driven by the radial gradient of the axial mean velocity. All other contributions to P_k vanish in the annular duct.

In the rotating case, the major contribution to turbulence production in the jet region comes from the eighth subterm $-\langle v'w'\rangle \langle w\rangle_{,r}$ in Eq. (1), which is caused by the rotating boundary layer, i.e., the radial gradient of the mean circumferential velocity. When the rotating boundary layer expands and the axial flow separates from the outer wall, the first and the seventh subterms become significant. The peak in the first subterm $-\langle u'u'\rangle \langle u\rangle_{,x}$ is caused by the separating axial flow,

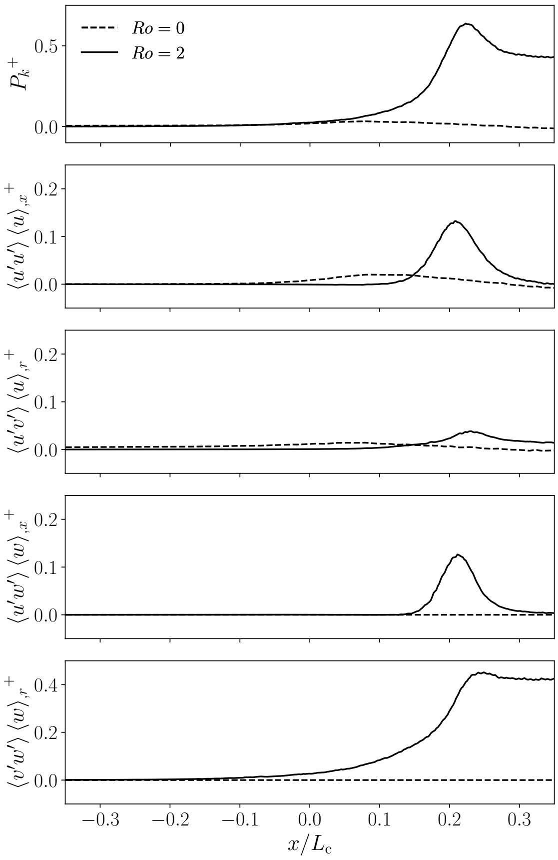

Figure 5: Axial profiles of production terms of TKE near the outer wall at $r/R = 0.98$. Complete production term P_k and selected subterms of Eq. (1).

which results in an axial gradient of the axial mean velocity. The peak in the seventh subterm $-\langle u'w' \rangle \langle w \rangle_{,x}$ is caused by the expanding rotating boundary layer, which results in an axial gradient of the circumferential mean velocity. In the annular duct, all contributions to the turbulence production vanish. Consequently, the flow laminarizes because no source of turbulence remains. Even the radial gradient of the axial mean velocity, which causes turbulence production in the non-rotating case, or the radial gradient of the circumferential mean velocity, has no effect here. The corresponding Reynolds shear stresses $\langle u'v' \rangle$ and $\langle v'w' \rangle$ are reduced to zero due to the rapid reduction of radial velocity fluctuations.

Vortex structures near the outer wall

Turbulent vortex structures in the outer part of the domain ($r/R > 0.5$) are illustrated in Fig. 6 for the non-rotating case (top) and the rotating case (bottom). The λ_2-criterion (Jeong & Hussain, 1995) is used to detect vortex structures in an arbitrary snapshot of the instantaneous flow. The structures are visualized by an isosurface of $\lambda_2/(R/U_p)^2 = -5000$. The isosurface is colored by the radial position. Near-wall structures are displayed in red, and structures close to the inner wall of the annular duct are colored blue. The section displayed in Fig. 6 covers the transition area between the jet region and the annular duct, where the relaminarization takes place.

In the jet region ($x > 0$), very small turbulent structures are visible in both cases, since the near-wall turbulent fluctuations have similar magnitude here. In the non-rotating case, the vortex structures become larger as the flow enters the annular duct and the bulk Reynolds number is reduced, but they remain close to the outer wall. In the rotating case, the vortex structures also increase in size. But in contrast to the former case, they are restricted to the inner part of the annular duct, and no vortices are detected anymore near the outer wall. This, again, illustrates the rapid relaminarization of the flow in the entrance region of the annular duct.

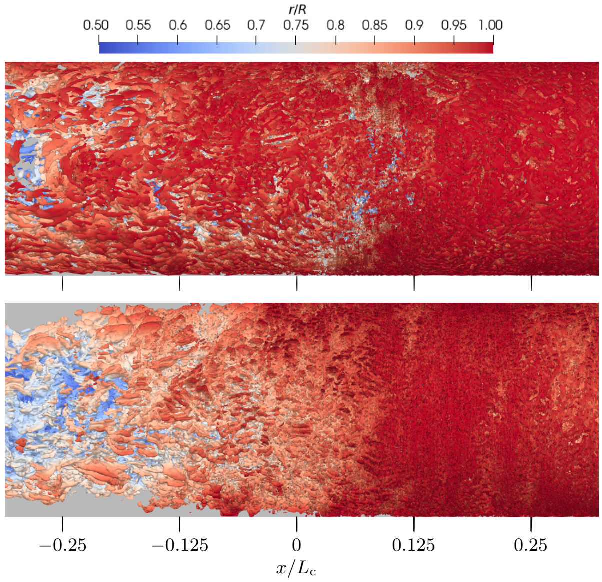

Figure 6: Vortex structures in the transition region near the outer wall visualized by an isosurface of λ_2-criterion. Top: $Ro = 0$, bottom: $Ro = 2$. The isosurface is colored by its radial position. Side view of the axisymmetric domain through the outer wall.

CONCLUSIONS

High-resolution large-eddy simulations were conducted employing a Fourier-spectral element method ($P = 10$) to investigate the influence of flow rotation on turbulence in a configuration relevant to rotor internal cooling of electric-vehicle drives. A rotating-wall case was compared with a non-rotating reference case. The general flow structure was characterized, and TKE profiles were reported to illustrate its development at representative locations in the domain. The rapid reduction in turbulence near the rotating outer wall can be explained by inspecting the production term in the TKE transport equation and its most significant contributions. Finally, the relaminarization was illustrated by visualizing the near-wall vortex structures.

Further analysis of the budget terms of the transport equation for the Reynolds stresses will be conducted in future studies to deepen the understanding of the mechanisms responsible for turbulence reduction in these regions. The locally enhanced or suppressed turbulence levels near the rotor wall are key to optimizing rotor internal cooling configurations.

ACKNOWLEDGMENT

The authors gratefully acknowledge the computing time made available to them on the high-performance computer at the NHR Center of TU Dresden. This center is jointly supported by the Federal Ministry of Research, Technology and

Space of Germany and the state governments participating in the NHR (www.nhr-verein.de/unsere-partner).

REFERENCES

Blackburn, H.M., Lee, D., Albrecht, T. & Singh, J. 2019 Semtex: A spectral element–Fourier solver for the incompressible Navier–Stokes equations in cylindrical or Cartesian coordinates. *Comput. Phys. Commun.* **245**, 106804.

Hultsch, T., Rüdiger, F., Stiller, J. & Fröhlich, J. 2023 Anisotropy and relaminarisation of the turbulent flow near a rotating cylindrical cavity wall. *Proc. Appl. Math. and Mech.* p. e202300263.

Hultsch, T., Stiller, J. & Fröhlich, J. in prep. A new radius-dependent kernel for the spectral vanishing viscosity method in cylindrical coordinates. Unpublished manuscript.

Imao, S., Itoh, M. & Harada, T. 1996 Turbulent characteristics of the flow in an axially rotating pipe. *Int. J. Heat Fluid Flow* **17** (5), 444–451.

Jeong, J. & Hussain, F. 1995 On the identification of a vortex. *J. Fluid Mech.* **285**, 69–94.

Koal, K., Stiller, J. & Blackburn, H.M. 2012 Adapting the spectral vanishing viscosity method for large-eddy simulations in cylindrical configurations. *J. Comput. Phys.* **231** (8), 3389–3405.

Maday, Y., Kaber, S.M.O. & Tadmor, E. 1993 Legendre Pseudospectral Viscosity Method for Nonlinear Conservation Laws. *SIAM J. Numer. Anal.* **30** (2), 321–342.

Nishibori, K., Kikuyama, K. & Murakami, M. 1987 Laminarization of turbulent flow in the inlet region of an axially rotating pipe. *JSME Int. J.* **30**, 255–262.

Orlandi, P. & Fatica, M. 1997 Direct simulations of turbulent flow in a pipe rotating about its axis. *J. Fluid Mech.* **343**, 43–72.

Schlatter, P. & Örlü, R. 2012 Turbulent boundary layers at moderate Reynolds numbers: inflow length and tripping effects. *J. Fluid Mech.* **710**, 5–34.

Tadmor, E. 1989 Convergence of spectral methods for nonlinear conservation laws. *SIAM J. Numer. Anal.* **26** (1), 30–44.

Weber, K. & Doerr, J. 2017 Elektrische Maschine sowie Verfahren zum Betreiben einer elektrischen Maschine.